High-Temperature Synthesis, Crystal Structure, and Properties of the New Sodium Rare-Earth Oxide Borates $Na_2RE_2(BO_3)_2O$ (*RE* = Dy, Ho)

Gunter Heymann, Konstantin Beyer, and Hubert Huppertz

Department Chemie und Biochemie, Ludwig-Maximilians-Universität München, Butenandtstraße 5 – 13 (Haus D), D-81377 München, Germany

Reprint requests to Priv.-Doz. Dr. H. Huppertz. E-mail: huh@cup.uni-muenchen.de

Z. Naturforsch. **59b,** 1200 – 1208 (2004); received July 20, 2004

Dedicated to Professor Hubert Schmidbaur on the occasion of his 70th birthday

The new monoclinic oxide borates $Na_2RE_2(BO_3)_2O$ (*RE* = Dy, Ho) were synthesized using standard solid-state reactions in the temperature range 900 – 950 °C. They are isotypic to the known phases $Na_2RE_2(BO_3)_2O$ (*RE* = Y, La, Nd, Sm-Gd, Er). The single crystal X-ray structure determination of $Na_2Dy_2(BO_3)_2O$ revealed: $P2_1/c$, $a = 1063.9(1)$, $b = 626.2(1)$, $c = 1025.3(1)$ pm, $\beta = 117.76(1)^\circ$, $Z = 4$, $R1 = 0.0221$, $wR2 = 0.0402$ (all data). The corresponding lattice parameters of $Na_2Ho_2(BO_3)_2O$ determined from powder data are $a = 1061.2(5)$, $b = 623.7(2)$, $c = 1022.5(3)$ pm, and $\beta = 117.7(1)^\circ$. The structure consists of infinite sheets of REO_8-polyhedra in the *bc*–plane, which are seperated by sodium atoms. The BO_3-groups are isolated forming layers in the *bc*-plane. The results of IR-spectroscopic investigations, temperature-resolved in-situ powder-diffraction measurements, and DTA/TG measurements on $Na_2Dy_2(BO_3)_2O$ are also presented.

Key words: Solid-State Synthesis, Oxide Borates, Crystal Structure

Introduction

In the last years, we paid attention to the synthesis of new oxoborates under high-pressure/high-temperature conditions, using a multianvil equipment, which enlarged our synthetical possibilities by an increased pressure and temperature range [1, 2]. The successful synthesis of new compounds in the field of rare-earth oxoborates, *e. g.* new high-pressure polymorphs like χ-*RE*BO_3 (*RE* = Dy, Er), which contain layers built up from non-cyclic $[B_3O_9]^{9-}$-anions [3] or new *meta*-oxoborates like β-*RE*$(BO_2)_3$ (*RE* = Dy-Lu) [4] and γ-*RE*$(BO_2)_3$ (*RE* = La-Nd) [5], led to new insights into the preparative possibilities under these extreme conditions. Especially the synthesis of compositions like $RE_4B_6O_{15}$ (*RE* = Dy, Ho) [6 – 8] and α-$RE_2B_4O_9$ (*RE* = Eu-Dy) [9, 10], where the new structural motif of edge-sharing BO_4-tetrahedra was observed for the first time, favoured systematic investigations in this field.

One of our aims was to search for quaternary phases in the system Na-Dy-B-O under high-pressure/high-temperature conditions. In contrast to an expected quaternary phase, our syntheses resulted in a new polymorph β-$Dy_2B_4O_9$, in which the added Na_2O_2 or Na_2CO_3 with a surplus of B_2O_3 acted as flux materials [11]. Therefore, we decided to synthesize a characterizable quaternary precursor material under ambient-pressure conditions, including the elements sodium, rare-earth, boron, and oxygen for a following transformation into a high-pressure polymorph.

Screening the literature for quaternary phases in the system Na-*RE*-B-O revealed compositions like $Na_3RE(BO_3)_2$ (*RE* = Y, La, Nd, Gd) [12, 13], $Na_{18}RE(BO_3)_7$ (*RE* = La, Nd) [14], and an oxide borate with the composition $Na_3La_9O_3(BO_3)_8$ [15], which exhibits La_9O_3-rings constituted of three La_4O-tetrahedra, sharing a common La corner. Furthermore, the phases $Na_3RE_2(BO_3)_3$ (*RE* = La, Nd, Sm) [14, 16, 17] were synthesized for detailed investigations of their nonlinear optical properties.

In 1999, Corbel *et al.* published the new isostructural family of oxide borates $Na_2RE_2(BO_3)_2O$ (*RE* = Sm, Eu, and Gd), hunting for new UV transparent materials with SHG (second harmonic generation) and/or laser properties [18]. They presented single crystal data for $Na_2Gd_2(BO_3)_2O$ (monoclinic structure, space group $P2_1/c$, $Z = 4$) and lattice parameters for $Na_2Sm_2(BO_3)_2O$ and $Na_2Eu_2(BO_3)_2O$. Ad-

0932–0776 / 04 / 1100–1200 $ 06.00

Table 1. Crystal data and structure refinement for $Na_2Dy_2(BO_3)_2O$.

Empirical formula	$Na_2Dy_2(BO_3)_2O$
Molar mass [g·mol^{-1}]	504.60
Crystal system	monoclinic
Space group	$P2_1/c$
Powder diffractometer	Stoe Stadi P
Radiation	Cu-K$_{\alpha1}$ ($\lambda = 154.06$ pm)
Powder diffraction data	
a [pm]	1064.1(2)
b [pm]	626.14(9)
c [pm]	1025.5(2)
β [°]	117.76(2)
Volume [Å^3]	604.7(1)
Single crystal diffractometer	Enraf-Nonius Kappa CCD
Radiation	Mo-K$_\alpha$ ($\lambda = 71.073$ pm)
Single crystal data	
a [pm]	1063.9(1)
b [pm]	626.2(1)
c [pm]	1025.3(1)
β [°]	117.76(1)
Volume [Å^3]	604.47(2)
Formula units per cell	$Z = 4$
Temperature [K]	293(2)
Calculated density [g·cm^{-3}]	5.545
Crystal size [mm^3]	$0.05 \times 0.06 \times 0.07$
Detector distance [mm]	40.0
Exposure time per deg [sec]	60
Absorption coefficient [mm^{-1}]	24.665
F(000)	880
θ Range [°]	4.0 to 35.0
Range in hkl	±17, ±10, ±16
Scan type	φ/ω
Total no. reflections	22164
Independent reflections	2657 ($R_{int} = 0.0560$)
Reflections with $I > 2\sigma(I)$	2466 ($R_\sigma = 0.0287$)
Data / parameters	2657 / 119
Absorption correction	numerical (HABITUS [24])
Goodness-of-fit (F^2)	1.158
Final R indices [$I > 2\sigma(I)$]	$R1 = 0.0181$
	$wR2 = 0.0395$
R Indices (all data)	$R1 = 0.0221$
	$wR2 = 0.0402$
Extinction coefficient	0.0032(2)
Larg. diff. peak a. hole [e·Å^{-3}]	2.3 / −2.4

ditionally, the authors performed luminescence investigations into Eu^{3+}-doped $Na_2Gd_2(BO_3)_2O$ at 77 K. In a later work (2000), Ivanova *et al.* illuminated the possibilities of synthesizing new members of this family with larger and smaller rare-earth cations [19]. In detail, they optimized the synthetic conditions of $Na_2RE_2(BO_3)_2O$ (*RE* = Y, La, Nd, and Er), taking two larger (La, Nd) and to smaller (Y, Er) rare-earth cations into account and presented crystallographic data from a Rietveld-refinement of a powder-sample from $Na_2Y_2(BO_3)_2O$. The authors concluded that the compounds with relatively small rare-earth cations can be synthesized successfully by solid-state reactions in the range 900 – 1000 °C in contrast to the syntheses with large rare-earth cations, which led to mixtures with other stable phases in this system. Recently, Zhang *et al.* reported photoluminescence properties of Eu^{3+}-doped $Na_2Y_2(BO_3)_2O$ [20].

Table 2. Atomic coordinates and isotropic equivalent displacement parameters U_{eq} [Å^2] for $Na_2Dy_2(BO_3)_2O$ (space group: $P2_1/c$). U_{eq} is defined as one third of the trace of the orthogonalized U_{ij} tensor.

Atom	Wyckoff-Position	x	y	z	U_{eq}
Dy1	4*e*	0.18397(2)	0.58203(2)	0.08832(2)	0.00756(4)
Dy2	4*e*	0.01688(2)	0.45939(2)	0.31821(2)	0.00718(4)
Na1	4*e*	0.5234(2)	0.4424(2)	0.2623(2)	0.0150(3)
Na2	4*e*	0.3898(2)	0.2613(3)	0.4530(2)	0.0194(3)
O1	4*e*	0.0276(2)	0.3748(3)	0.9043(2)	0.0089(4)
O2	4*e*	0.8322(2)	0.2610(3)	0.1349(2)	0.0094(4)
O3	4*e*	0.1488(2)	0.9582(3)	0.0863(2)	0.0107(4)
O4	4*e*	0.1498(2)	0.2585(3)	0.2283(2)	0.0109(4)
O5	4*e*	0.3175(2)	0.2444(4)	0.1359(3)	0.0126(4)
O6	4*e*	0.3967(2)	0.6618(4)	0.0542(2)	0.0131(4)
O7	4*e*	0.3693(2)	0.6501(4)	0.3369(2)	0.0135(4)
B1	4*e*	0.2086(3)	0.1524(5)	0.1493(3)	0.0087(5)
B2	4*e*	0.3156(3)	0.7503(5)	0.9181(3)	0.0095(5)

In this paper, we describe the syntheses of the new rare-earth oxide borates $Na_2RE_2(BO_3)_2O$ with *RE* = Dy and Ho, followed by a detailed structural characterization of the dysprosium-phase including its thermal properties. That way we get a well characterized compound (precursor) for the intended high-pressure/high-temperature investigations in the quaternary system Na-Dy-B-O, using $Na_2Dy_2(BO_3)_2O$ as starting material.

Experimental Section

According to eq. (1), the compounds $Na_2RE_2(BO_3)_2O$ (*RE* = Dy, Ho) were synthesized by standard solid-state reactions using molar mixtures of RE_2O_3 (*RE* = Dy, Ho; purity > 99.9%, Sigma-Aldrich, Taufkirchen), Na_2CO_3 (purity > 99.9%, Merck, Darmstadt), and H_3BO_3 (purity > 99.8%, Merck, Darmstadt). Additionally, an amount of three mole Na_2CO_3 was added as flux-material. All starting materials were mixed thoroughly under air using an agate mortar.

$$RE_2O_3 + 2\,H_3BO_3 + Na_2CO_3 \xrightarrow[900-950\,^\circ C]{Na_2CO_3\text{-Flux}} Na_2RE_2(BO_3)_2O + 3\,H_2O + CO_2 \quad (RE = \mathrm{Dy, Ho}) \qquad (1)$$

The starting materials were filled into a zirconia crucible, which was positioned inside a standard quartz-ampoule. To

Table 3. Anisotropic displacement parameters [Å^2] for $Na_2Dy_2(BO_3)_2O$ (space group: $P2_1/c$).

Atom	U_{11}	U_{22}	U_{33}	U_{23}	U_{13}	U_{12}
Dy1	0.00744(6)	0.00703(6)	0.00798(6)	−0.00009(4)	0.00341(5)	−0.00016(4)
Dy2	0.00842(6)	0.00616(6)	0.00750(6)	−0.00001(4)	0.00417(5)	−0.00034(4)
Na1	0.0136(6)	0.0132(6)	0.0166(6)	0.0017(5)	0.0057(5)	−0.0014(5)
Na2	0.0140(6)	0.0283(8)	0.0162(7)	−0.0033(6)	0.0073(5)	−0.0001(5)
O1	0.0107(9)	0.0077(9)	0.0089(9)	−0.0017(7)	0.0052(7)	−0.0009(7)
O2	0.0076(8)	0.0100(9)	0.0098(9)	−0.0011(7)	0.0034(7)	−0.0001(7)
O3	0.014(2)	0.0083(9)	0.012(2)	−0.0007(7)	0.0074(8)	−0.0012(7)
O4	0.0124(9)	0.0095(9)	0.013(2)	−0.0015(7)	0.0079(8)	−0.0003(7)
O5	0.0094(9)	0.013(2)	0.018(2)	0.0008(8)	0.0084(8)	−0.0001(8)
O6	0.011(2)	0.016(2)	0.011(2)	0.0040(8)	0.0043(8)	0.0015(8)
O7	0.013(2)	0.016(2)	0.011(2)	−0.0037(8)	0.0057(8)	0.0010(8)
B1	0.011(2)	0.006(2)	0.008(2)	0.000(2)	0.004(2)	−0.000(2)
B2	0.009(2)	0.010(2)	0.009(2)	0.001(2)	0.004(2)	0.001(2)

Table 4. Interatomic distances [pm] calculated with the single crystal lattice parameters in $Na_2Dy_2(BO_3)_2O$ (Standard deviations in parentheses).

Dy1-O1a	225.6(2)	Dy2-O1b	225.4(2)	Na1-O5a	231.7(3)	Na2-O5b	233.6(3)
Dy1-O1b	230.3(2)	Dy2-O2a	234.5(2)	Na1-O6a	236.2(3)	Na2-O6a	238.9(3)
Dy1-O3	238.4(2)	Dy2-O1a	234.5(2)	Na1-O6b	242.0(3)	Na2-O4	251.9(3)
Dy1-O2	242.2(2)	Dy2-O4a	237.6(2)	Na1-O5b	242.6(3)	Na2-O7a	252.5(3)
Dy1-O7	242.6(2)	Dy2-O2b	237.9(2)	Na1-O7a	247.6(3)	Na2-O7b	267.4(3)
Dy1-O5	246.6(2)	Dy2-O3a	238.2(2)	Na1-O7b	260.2(3)	Na2-O6b	283.4(3)
Dy1-O6	249.7(2)	Dy2-O4b	246.8(2)			Na2-O5a	297.4(3)
Dy1-O4	260.5(2)	Dy2-O3b	249.0(2)				
	⌀242.0		⌀238.0		⌀243.4		⌀260.7
				O1-Dy1a	225.6(2)		
B1-O3	138.4(4)	B2-O7	136.1(4)	O1-Dy1b	230.3(3)		
B1-O4	140.1(4)	B2-O2	140.6(4)	O1-Dy2a	225.4(2)		
B1-O5	135.7(4)	B2-O6	137.1(4)	O1-Dy2b	234.5(2)		
	⌀138.1		⌀137.9		⌀229.0		

prevent reactions between the crucible and the wall of the ampoule, the zirconia crucible was outside coated with a nickel foil. For the dysprosium phase, the resistance furnace was heated up to 900 °C in steps of 1 °C per minute and to 950 °C for the synthesis of $Na_2Ho_2(BO_3)_2O$, respectively. In the case of $Na_2Dy_2(BO_3)_2O$, the temperature was hold for 8 days, followed by slow cooling (1 °C/min) to room temperature. This procedure led to a nearly single phase, colourless, crystalline product. By the X-ray powder diffraction pattern a small amount of Dy_2O_3 was identified as a byproduct. Quantitative analytical investigations, using energy dispersive X-ray analysis (EDX), confirmed the ratio Na:Dy = 1:1.

For the synthesis of $Na_2Ho_2(BO_3)_2O$, the temperature of 950 °C was hold for 17 hours, leading to a mixture of $Na_2Ho_2(BO_3)_2O$ and a new phase, which has not been identified until now. In analogy to former characterized phases, containing the rare-earth element holmium, we observed different colours of $Na_2Ho_2(BO_3)_2O$. In daylight, the crystals show a light beige colour, while indoors (neon lamps) they appear bright pink (Alexandrite-effect) [21].

Crystal Structure Analysis

The powder diffraction data of the monoclinic compounds $Na_2RE_2(BO_3)_2O$ (*RE* = Dy, Ho) were collected on a STOE Stadi P diffractometer with monochromatized Cu-$K_{\alpha 1}$ radiation. The diffraction pattern of $Na_2Dy_2(BO_3)_2O$ was indexed with the program ITO [22] on the basis of a monoclinic unit cell. The lattice parameters $a = 1064.1(2)$, $b = 626.14(9)$, $c = 1025.5(2)$ pm, and $\beta = 117.76(2)^\circ$ (Table 1) were obtained from least-squares fits of the powder data. The correct indexing of the pattern was confirmed by intensity calculations [23], taking the atomic positions from the structure refinements for $Na_2Dy_2(BO_3)_2O$. The lattice parameters, determined from the powder and the single crystal, agree well. Indexing the diffraction pattern of $Na_2Ho_2(BO_3)_2O$, we got the following lattice parameters: $a = 1061.2(5)$, $b = 623.7(2)$, $c = 1022.5(3)$ pm, and $\beta = 117.7(1)^\circ$.

Some small single crystals of $Na_2Dy_2(BO_3)_2O$ were isolated by mechanical fragmentation and examined by Buerger precession photographs. The single crystal intensity data were collected from a regularly shaped colorless crystal at room temperature by use of an Enraf-Nonius Kappa CCD, equipped with a rotating anode [Mo-K_α radiation (71.073 pm)]. A numerical absorption correction (HABITUS [24]) was applied to all data. All relevant information of the data collection is listed in Table 1. According to the systematic

Table 5. Interatomic angles [°] calculated with the single crystal lattice parameters in $Na_2Dy_2(BO_3)_2O$ (Standard deviations in parentheses).

O5-B1-O3	123.7(3)	O7-B2-O6	124.3(3)	Dy2-O1-Dy1	138.2(2)
O5-B1-O4	119.3(3)	O7-B2-O2	120.0(3)	Dy2-O1-Dy1	104.5(1)
O3-B1-O4	117.0(3)	O6-B2-O2	115.7(3)	Dy1-O1-Dy1	104.9(1)
	⌀120.0		⌀120.0	Dy2-O1-Dy2	94.6(1)
				Dy1-O1-Dy2	107.2(1)
				Dy1-O1-Dy2	102.9(1)
					⌀108.7

extinctions $h0l$ with $l = 2n$, $0k0$ with $k = 2n$, and $00l$ with $l = 2n$ the space group $P2_1/c$ (No. 14) was derived. The starting positional parameters were deduced from an automatic interpretation of direct methods with SHELXS-97 [25]. A successful refinement with anisotropic displacement parameters using SHELXL-97 [26] (full-matrix least-squares on F^2) was possible for all atoms. The final difference Fourier syntheses revealed no significant residual peaks in the refinement (Table 1). All relevant parameters for the intensity data collection of the dysprosium-phase are listed in Table 1. The positional parameters, anisotropic displacement parameters, interatomic distances, and angles of the final refinement are listed in the Tables 2 – 5. Further details for $Na_2Dy_2(BO_3)_2O$ are available from the Fachinformationszentrum Karlsruhe, D-76344 Eggenstein-Leopoldshafen (Germany), email: crysdata@fiz-karlsruhe.de, by quoting the registry number CSD-414226.

Results and Discussion

The crystal structures of $Na_2RE_2(BO_3)_2O$ (*RE* = Dy, Ho) are isotypic to the former published compounds $Na_2RE_2(BO_3)_2O$ (*RE* = Y, La, Nd, Sm-Gd, Er) [18, 19]. Therefore, the structure will be described just briefly, emphasizing structural aspects, which were not described until now. Figure 1 shows the crystal structure of $Na_2RE_2(BO_3)_2O$ (*RE* = Dy, Ho) (view along [010]), exhibiting isolated triangular BO_3-groups, which share edges and corners with the polyhedra of the rare-earth and sodium atoms. In detail, the grey $RE(1)O_8$-polyhedra form $RE(1)_2O_{14}$-dimers (Fig. 1). These dimers are inserted into a sheet of $RE(2)O_8$-polyhedra (white), which lies in the *bc*-plane (Fig. 2, right). The $RE(2)O_8$-polyhedra are connected *via* common edges along *c* and *via* triangular faces along *b*. As Corbel *et al.* [18] pointed out, this structural motif was also observed in ThI_4, where similar layers of distorted ThI_8 antiprisms were found [27].

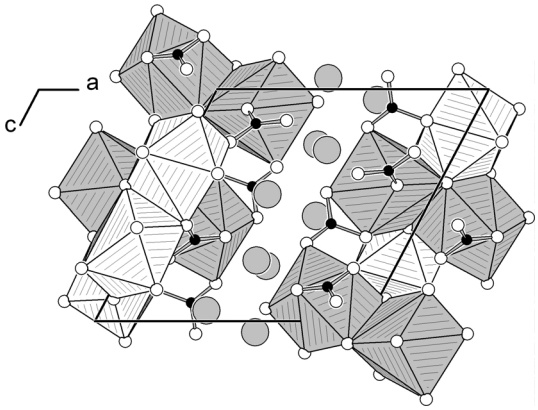

Fig. 1. Crystal structure of the monoclinic sodium rare-earth oxide borates $Na_2RE_2(BO_3)_2O$ (*RE* = Dy, Ho), view along [010]. The $RE(1)O_8$-polyhedra appear grey and the $RE(2)O_8$-polyhedra white. Sodium atoms are represented by grey spheres, oxygen and boron atoms by white and small black spheres, respectively.

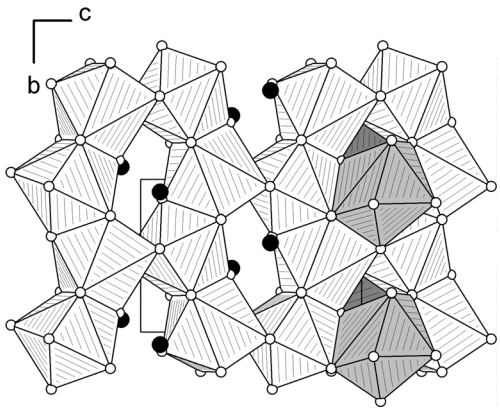

Fig. 2. Connection of the $RE(2)O_8$-polyhedra (*RE* = Dy, Ho) (white) inside the *bc*-plane with inserted $RE(1)_2O_{14}$-dimers (*RE* = Dy, Ho) (grey). For a better understanding of the structure, the grey dimers are only inserted on the right side of this illustration.

In $Na_2RE_2(BO_3)_2O$ (*RE* = Dy, Ho), the connection between the two different rare-earth-polyhedra takes place *via* common edges. Along *a*, these sheets are separated by sodium atoms (grey spheres in Fig. 1). The sodium atoms are coordinated by six (Na(1)) and seven oxygen atoms (Na(2)). The distorted $Na(1)O_6$-octahedra (white) are connected to chains *via* common faces along *b*. Figure 3 shows, how these chains share common faces with the $Na(2)O_7$-polyhedra (grey), leading to a layer in the *bc*-plane. Figure 4 gives another view of the crystal structure of $Na_2RE_2(BO_3)_2O$ (*RE* = Dy, Ho), emphasizing the layer of distorted

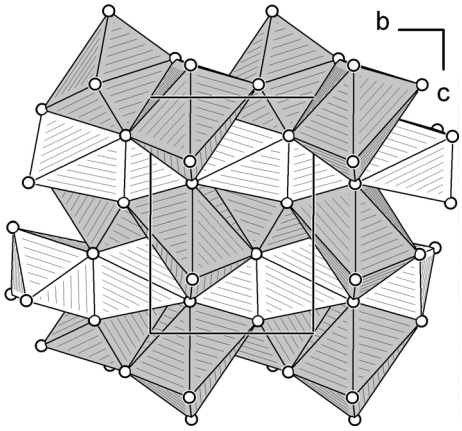

Fig. 3. Connection between the distorted $Na(1)O_6$-octahedra (white) and the $Na(2)O_7$-polyhedrons (grey) in the *bc*-plane.

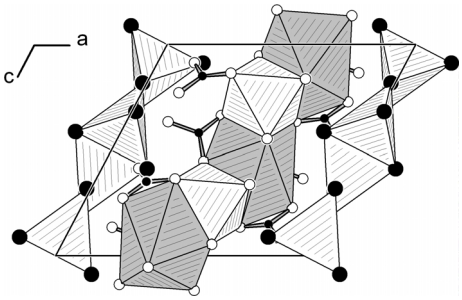

Fig. 4. Crystal structure of the monoclinic sodium rare-earth oxide borates $Na_2RE_2(BO_3)_2O$ (*RE* = Dy, Ho), view along [010]. The distorted $Na(1)O_6$-octahedra are shown as white polyhedra, whereas the $Na(2)O_7$-polyhedra appear grey. Additionally, the distorted ORE_4-tetrahedra (white polyhedra with large black spheres (*RE*)) are drawn.

$Na(1)O_6$-octahedra (white) and $Na(2)O_7$-polyhedra (grey) in the middle, flanked on each side by RE_4O-tetrahedra. In contrast to Fig. 1, this representation is accentuated by the coordination polyhedra RE_4O of the single oxygen atom O(1), which is not bonded with boron. Figure 5 demonstrates the layer built up from corner- and edge-sharing RE_4O-tetrahedra inside the *bc*-plane. Due to the large size of the oxygen atoms and their rather low charge, corner- and edge-sharing of oxocentred tetrahedra $[OM_4]$ can be found in several crystal structures of inorganic compounds [28].

All triangular BO_3-groups are isolated forming layers in the *bc*-plane, in which one half is standing at the base and the other half is standing at the top (Fig. 6). The B-O bond-lengths inside the BO_3-groups of $Na_2Dy_2(BO_3)_2O$ vary between 135 and 141 pm with an average value of 138.0 pm, which corresponds to the

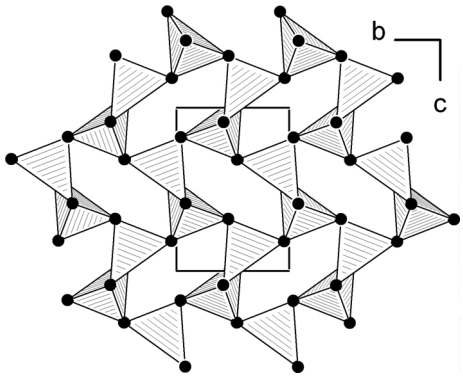

Fig. 5. Layer of corner- and edge-sharing RE_4O-tetrahedra (*RE* = Dy, Ho) inside the *bc*-plane of $Na_2RE_2(BO_3)_2O$ (*RE* = Dy, Ho).

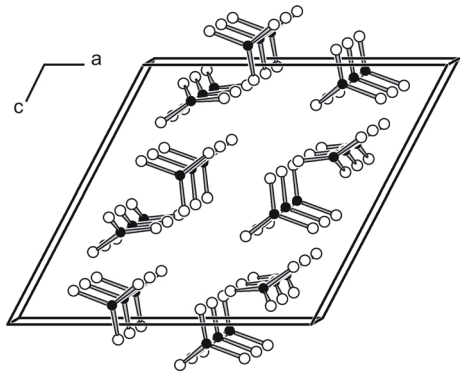

Fig. 6. Ordering of the BO_3-groups in the crystal structure of $Na_2RE_2(BO_3)_2O$ (*RE* = Dy, Ho), view along [010].

known value of 137.0 pm for oxoborates within BO_3-groups [29, 30]. The Dy-O distances inside the two different DyO_8-polyhedra (Fig. 7) vary between 225 and 261 pm with an average value of 240 pm (Table 4). Due to the smaller size of the dysprosium-cation, the distances are slightly shorter than the Gd-O distances in the isotypic compound $Na_2Gd_2(BO_3)_2O$, which vary between 228 and 262 pm [18]. The distances Na-O range from 231 – 260 pm inside the distorted $Na(1)O_6$-octahedra and from 233 – 297 pm in the $Na(2)O_7$-polyhedra (Fig. 8 and Table 4), which correspond to the values found in $Na_2Gd_2(BO_3)_2O$ (Na1: 233 – 263 pm; Na2: 235 – 300 pm) [18] and $Na_2Y_2(BO_3)_2O$ (Na1: 224 – 273 pm; Na2: 239 – 299 pm) [19]. Inside the distorted Dy_4O-tetrahedra, the Dy-O1 distances vary between 225 – 235 pm. These values agree with the data found for the centred rare-earth tetrahedron in $Na_2Gd_2(BO_3)_2O$ (228 – 236 pm) [18], taking into account the larger size of Gd^{3+}.

Table 6. Charge distribution in $Na_2Dy_2(BO_3)_2O$, calculated with the bond-length/bond-strength concept (ΣV) [31, 32] and the CHARDI concept (ΣQ) [33].

	Dy1	Dy2	Na1	Na2	O1	O2	O3	O4	O5	O6	O7	B1	B2
ΣQ	+3.02	+3.02	+0.99	+1.00	−1.94	−2.04	−2.03	−1.95	−2.10	−1.98	−1.96	+2.96	+3.01
ΣV	+2.91	+3.17	+1.10	+0.91	−2.00	−2.07	−2.02	−1.97	−2.00	−1.94	−1.87	+2.90	+2.92

Table 7. Cell parameters of the sodium rare-earth oxide borates $Na_2RE_2(BO_3)_2O$.

Oxide borate	*a* [pm]	*b* [pm]	*c* [pm]	β [°]	*V* [Å^3]	Reference
$Na_2Y_2(BO_3)_2O$	1059.78(3)	623.04(3)	1022.41(6)	117.76(3)	593.37(6)	[19]
$Na_2Nd_2(BO_3)_2O$	1082.04(7)	642.97(6)	1046.17(9)	117.96(3)	642.87(9)	[19]
$Na_2Sm_2(BO_3)_2O$	1075.4(2)	636.9(2)	1038.1(2)	117.85(2)	628.6(2)	[18]
$Na_2Eu_2(BO_3)_2O$	1072.1(7)	634.3(6)	1034.7(7)	117.84(5)	622.1(6)	[18]
$Na_2Gd_2(BO_3)_2O$	1069.5(6)	632.0(4)	1032.8(6)	117.80(4)	617.5(9)	[18]
$Na_2Dy_2(BO_3)_2O$	1063.9(1)	626.2(1)	1025.3(1)	117.76(1)	604.47(2)	this work
$Na_2Ho_2(BO_3)_2O$	1061.2(5)	623.7(2)	1022.5(3)	117.7(1)	599.0(5)	this work
$Na_2Er_2(BO_3)_2O$	1057.57(2)	620.99(2)	1019.75(2)	117.74(2)	592.7(2)	[19]

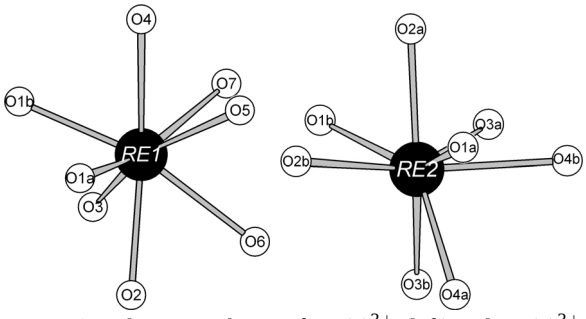

Fig. 7. Coordination spheres of $RE(1)^{3+}$ (left) and $RE(2)^{3+}$ (right) in the crystal structure of $Na_2RE_2(BO_3)_2O$ (*RE* = Dy, Ho).

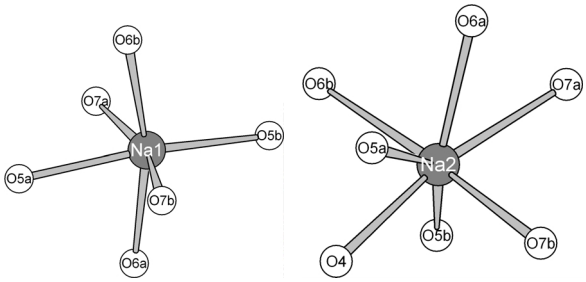

Fig. 8. Coordination spheres of $Na(1)^+$ (left) and $Na(2)^+$ (right) in the crystal structure of $Na_2RE_2(BO_3)_2O$ (*RE* = Dy, Ho).

For further clarification, we calculated bond-valence sums for $Na_2Dy_2(BO_3)_2O$ with the bond-length/bond-strength concept and the CHARDI concept (Table 6) [31–33]. The formal ionic charges of the atoms, acquired by the results of the X-ray structure analysis, are in agreement within the limits of the concepts. Additionally, we calculated MAPLE values (**Ma**delung **P**art of **L**attice **E**nergy) [34–36] for $Na_2Dy_2(BO_3)_2O$ to compare them with the MAPLE value of the binary components Dy_2O_3, Na_2O and the normal-pressure modification B_2O_3-I [Dy_2O_3 (15199 kJ mol^{-1}) + B_2O_3-I (21924 kJ mol^{-1}) + Na_2O (2912 kJ mol^{-1})]. The deviation of the calculated value of 39945 kJ mol^{-1} comes to 0.2% in comparison to the MAPLE value obtained from the binary oxides (40035 kJ mol^{-1}).

In order to compare the lattice parameters of $Na_2RE_2(BO_3)_2O$ (*RE* = Dy, Ho) with those of the isotypic compounds, we summarized all data in Table 7 and Fig. 9. These data clearly show the lanthanoid contraction. For the lanthanum compound, lattice parameters were not available.

Infrared spectroscopy

The infrared (IR) spectrum of $Na_2Dy_2(BO_3)_2O$ (Fig. 10) was recorded on a Bruker IFS66/v spectrometer, scanning a range from 400 to 4000 cm^{-1}. The samples were thoroughly mixed with dried KBr (5 mg sample, 500 mg KBr) in a glove box under dried argon atmosphere. Figure 10 shows the section 400–2000 cm^{-1} of the infrared spectrum. Generally, isolated planar BO_3-groups with trigonal symmetry exhibit four fundamental modes of vibration [37]: the symmetric stretching ($\nu_1 = 900 - 1000$ cm^{-1}), the out of plane bending ($\nu_2 = 700 - 780$ cm^{-1}), the antisymmetric stretching ($\nu_3 = 1100 - 1300$ cm^{-1}), and the in plane bending ($\nu_4 = 590 - 680$ cm^{-1}). Both, ν_3 and ν_4 are doubly degenerated and ν_1 is ordinarily inactive in the infrared. Due to the crystalline environment, ν_1 may become active and the degeneracy of the out of plane (ν_3) and in plane (ν_4) vibration can be removed.

Having a look at the recorded IR-spectrum (Fig. 10) and keeping the above mentioned restrictions in mind,

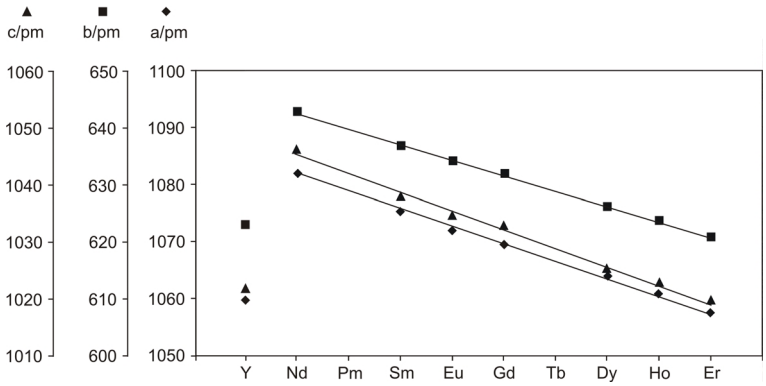

Fig. 9. Plot of the lattice parameters of the monoclinic sodium rare-earth oxide borates $Na_2RE_2(BO_3)_2O$ (*RE* = Nd, Sm-Gd, Dy-Er).

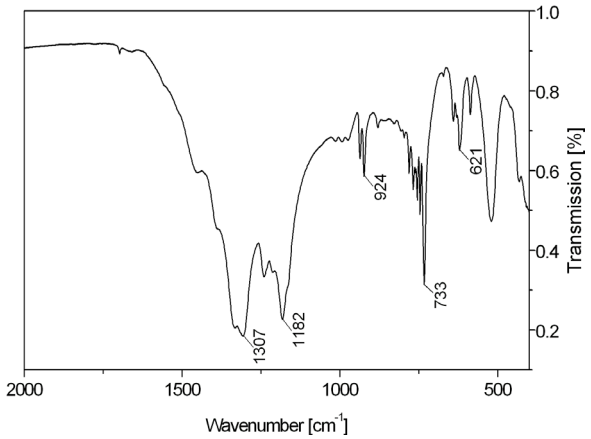

Fig. 10. IR-spectrum of $Na_2Dy_2(BO_3)_2O$.

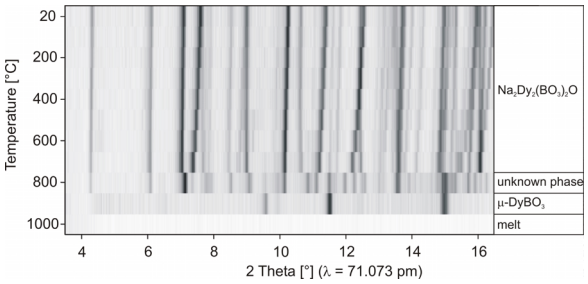

Fig. 11. Temperature-dependent X-ray powder patterns of $Na_2Dy_2(BO_3)_2O$.

it can be concluded that the strong, broad absorptions in the region 1170 to 1400 cm^{-1} correspond to the asymmetric stretching vibrations (ν_3) of the BO_3-groups. These bands belong to the strongest and most prominent features of the spectrum. In addition, the strong and usually sharp absorptions derived from the out of plane bending (ν_2) of the trigonal ion occur in the range 730 – 790 cm^{-1}. The absorptions between 600 – 650 cm^{-1} are attributed to the in plane bending (ν_4) of the BO_3-groups. According to the crystalline environment, the vibrations in the range 920 – 940 cm^{-1} can presumably be classified as symmetric stretching vibrations.

The recorded IR spectrum confirms the presence of BO_3-groups in the crystal structure of $Na_2Dy_2(BO_3)_2O$. Due to two crystallographically different BO_3-groups and crystal field effects, the absorptions in the spectrum are split. In the upper range (4000 – 2000 cm^{-1}) no absorption bands due to hydrogen (OH) were detectable.

In-situ powder diffraction and thermoanalytical measurements

To investigate the high-temperature behaviour of the new phase $Na_2Dy_2(BO_3)_2O$, temperature dependent in-situ X-ray diffractometry was performed on a STOE powder diffractometer Stadi P (Mo-K_α; λ = 71.073 pm) with a computer-controlled STOE furnace. An electrically heated graphite tube held the sample capillary vertical with respect to the scattering plane. Bores in the graphite tube permitted unobstructed pathways for the primary beam as well as for the scattered radiation. The temperature, measured by a thermocouple in the graphite tube, was kept constant within 0.2 °C. The heating rate between different temperatures was set to 22 °C/min. For temperature stabilization, a time of three minutes was allowed before starting each data acquisition. Successive heating of $Na_2Dy_2(BO_3)_2O$ (Fig. 11) shows, that the room temperature modification is stable up to a temperature of 700 °C. Further heating in the range of 700 – 800 °C led to a transformation into a new unidentified phase. Following heating in the area 800 – 900 °C resulted in a decomposition into the high-temperature

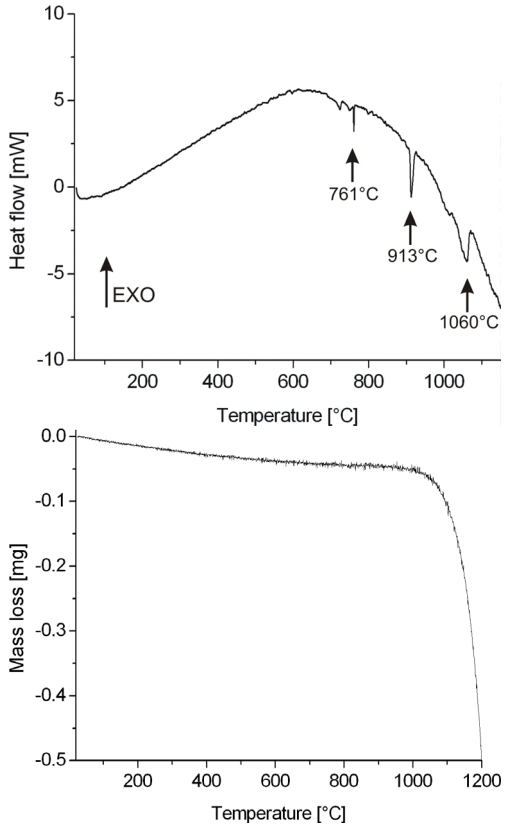

Fig. 12. Differential thermal analysis curve (top) and thermogravimetrical behaviour (bottom) of $Na_2Dy_2(BO_3)_2O$.

orthoborate μ-$DyBO_3$ [38]. This agrees with observations of Ivanova *et al.*, who pointed out, that even if the solid-state reactions led to the formation of the oxide borates $Na_2RE_2(BO_3)_2O$, they melt incongruently [19]. The only exception was $Na_2Nd_2(BO_3)_2O$, which was assumed to melt congruently at 1190 °C. For $Na_2Dy_2(BO_3)_2O$ it was not possible to detect a crystalline phase at 1000 °C. Subsequent cooling to room temperature revealed no further reflections due to the formation of a glass. In contrast to former in-situ powder diffraction studies of ternary systems like χ-$DyBO_3$ [3], β-$Dy_2B_4O_9$ [11], and $Dy_4B_6O_{15}$ [7], where it was still possible to detect μ-$DyBO_3$ [38] at 1000 °C, the portion of sodium oxide leads to an earlier melting of μ-$DyBO_3$.

These results were confirmed by thermoanalytical measurements, which were performed with a combined DTA-TG-thermobalance (TGA 92-2400, Setaram, heating rate: 10 °C min^{-1}) between room temperature and 1200 °C (Fig. 12). While heating, two sharp endothermic effects (maxima at 761 °C and 913 °C) and a relatively broad one (start at about 1000 °C, maximum at 1060 °C) occured in the DTA, which can be attributed to the transformation into the unidentified phase (761 °C), the decomposition into μ-$DyBO_3$ [38] (913 °C), and melting above 1000 °C. Additionally, we observed a weight-loss starting at approx. 1000 °C due to the evaporation of the decomposition products like boron oxide (starting weight: 18.088 mg).

Conclusions

In this paper we described the syntheses of the new rare-earth oxide borates $Na_2RE_2(BO_3)_2O$ with *RE* = Dy, Ho. These compounds enlarge the series of isotypic compounds by two other members. Former experiments to synthesize a quaternary compound under high-pressure/high-temperature conditions in the system Na-Dy-B-O, starting from the oxides, resulted always in the formation of ternary compounds. With $Na_2Dy_2(BO_3)_2O$, we synthesized a precursor material, which may allow the access into a quaternary high-pressure phase in the future.

Acknowledgements

We gratefully acknowledge the continous support of these investigations by Prof. Dr. W. Schnick, Department Chemie and Biochemie of the Ludwig-Maximilians-Universität München (Germany). Special thanks go to Dr. P. Mayer and S. Albrecht (LMU-München) for collecting the single-crystal data, to Dipl.-Min. S. Schmid for DTA/TG, and to Dipl.-Chem. S. Correll (LMU-München) for the in-situ powder diffraction measurements. This work was financially supported by the Deutsche Forschungsgemeinschaft and the European COST D30 network (D30/003/03).

[1] H. Huppertz, Z. Naturforsch. **56b**, 697 (2001).
[2] H. Huppertz, Z. Kristallogr. **219**, 330 (2004).
[3] H. Huppertz, B. von der Eltz, R.-D. Hoffmann, H. Piotrowski, J. Solid State Chem. **166**, 203 (2002).
[4] H. Emme, T. Nikelski, Th. Schleid, R. Pöttgen, M. H. Möller, H. Huppertz, Z. Naturforsch. **59b**, 202 (2004).
[5] H. Emme, C. Despotopoulou, H. Huppertz, Z. Anorg. Allg. Chem. **630**, (2004) in press.
[6] H. Huppertz, B. von der Eltz, J. Am. Chem. Soc. **124**, 9376 (2002).
[7] H. Huppertz, Z. Naturforsch. **58b**, 278 (2003).

[8] H. Huppertz, H. Emme, J. Phys.: Condens. Matter **16**, S1283 (2004).
[9] H. Emme, H. Huppertz, Z. Anorg. Allg. Chem. **628**, 2165 (2002).
[10] H. Emme, H. Huppertz, Chem. Eur. J. **9**, 3623 (2003).
[11] H. Huppertz, S. Altmannshofer, G. Heymann, J. Solid State Chem. **170**, 320 (2003).
[12] J. Mascetti, M. Vlasse, C. Fouassier, J. Solid State Chem. **39**, 288 (1981).
[13] Y. Zhang, X. L. Chen, J. K. Liang, T. Xu, J. Alloys Compd. **333**, 72 (2002).
[14] J. Mascetti, C. Fouassier, P. Hagenmuller, J. Solid State Chem. **50**, 204 (1983).
[15] P. Gravereau, J.-P. Chaminade, S. Pechev, V. Nikolov, D. Ivanova, P. Pechev, Solid State Sci. **4**, 993 (2002).
[16] G. Zhang, Y. Wu, P. Fu, G. Wang, S. Pan, C. Chen, Chem. Lett. **30**, 456 (2001).
[17] G. Zhang, Y. Wu, P. Fu, G. Wang, H. Liu, G. Fan, C. Chen, J. Phys. Chem. Solids **63**, 145 (2002).
[18] G. Corbel, M. Leblanc, E. Antic-Fidancev, M. Lemaître-Blaise, J. Solid State Chem. **144**, 35 (1999).
[19] D. I. Ivanova, S. P. Pechev, V. S. Nikolov, P. D. Peshev, Bulg. Chem. Commun. **32**, 409 (2000).
[20] Y. Zhang, Y. D. Li, J. Alloys Compd. **370**, 99 (2004).
[21] H. M. Farok, G. A. Saunders, W. A. Lambsom, R. Krüger, H. B. Senin, S. Bartlett, S. Takel, Phys. Chem. Glasses **37**, 125 (1996).
[22] J. W. Visser, J. Appl. Crystallogr. **2**, 89 (1969).
[23] WinX^{POW} Software, STOE & CIE GmbH, Darmstadt (1998).
[24] W. Herrendorf, H. Bärnighausen, HABITUS, Program for Numerical Absorption Correction, University of Karlsruhe / Giessen, Germany (1993 / 1997).
[25] G. M. Sheldrick, SHELXS-97, Program for the Solution of Crystal Structures, University of Göttingen, Germany (1997).
[26] G. M. Sheldrick, SHELXL-97, Program for Crystal Structure Refinement, University of Göttingen, Germany (1997).
[27] A. Zalkin, J. D. Forrester, D. H. Templeton, Inorg. Chem. **3**, 639 (1964).
[28] S. V. Krivovichev, S. K. Filatov, T. F. Semenova, Russ. Chem. Rev. **67**, 137 (1998).
[29] F. C. Hawthorne, P. C. Burns, J. D. Grice, Boron: Mineralogy, Petrology, and Geochemistry, Chapter 2, Reviews in Mineralogy 33, Mineralogical Society of America, Washington (1996).
[30] E. Zobetz, Z. Kristallogr. **160**, 81 (1982).
[31] I. D. Brown, D. Altermatt, Acta Crystallogr. Sect. B **41**, 244 (1985).
[32] N. E. Brese, M. O'Keeffe, Acta Crystallogr. Sect. B **47**, 192 (1991).
[33] R. Hoppe, S. Voigt, H. Glaum, J. Kissel, H. P. Müller, K. Bernet, J. Less-Common Met. **156**, 105 (1989).
[34] R. Hoppe, Angew. Chem. **78**, 52 (1966); Angew. Chem. Int. Ed. Engl. **5**, 95 (1966).
[35] R. Hoppe, Angew. Chem. **82**, 7 (1970); Angew. Chem. Int. Ed. Engl. **9**, 25 (1970).
[36] R. Hübenthal, MAPLE, Program for the Calculation of MAPLE Values, Vers. 4, University of Gießen, Germany (1993).
[37] C. E. Weir, R. A. Schroeder, J. Research NBS **68A**, 465 (1964).
[38] E. M. Levin, R. S. Roth, J. B. Martin, Am. Mineral. **46**, 1030 (1961).